Soft Matter

Dynamic Article Links

Cite this: *Soft Matter*, 2012, **8**, 3596

www.rsc.org/softmatter

PAPER

Electrokinetics of concentrated suspensions of spheroidal hematite nanoparticles

Raúl A. Rica,†* María L. Jiménez and Ángel V. Delgado

Received 13th December 2011, Accepted 16th January 2012
DOI: 10.1039/c2sm07365j

The effect of the volume fraction of solids on the concentration polarization around spheroidal particles has been recently investigated using data on the low frequency dielectric dispersion (LFDD) of suspensions [Rica *et al.*, *Soft Matter*, 2011, **7**, 3286]. In this work, we extend our previous experimental analysis including new measurements at different surface charge together with dynamic electrophoretic mobility determinations. This joint study allows us to detect two α relaxations, due to the two characteristic dimensions of our rod-like particles, in addition to the Maxwell–Wagner–O'Konski relaxation and the inertial effects on the electrophoretic mobility. Available theoretical models for the polarization of a single rod are extended to consider particle–particle interactions, this leading to the estimation of the zeta potential and the characteristic size and geometry of the particles. The most significant result of the LFDD experiments is the different trend of low and high frequency relaxations with volume fraction. Calculation of the concentration polarization maps around the spheroidal particle suggests that such different trends can be explained by the different extent of the polarization clouds along both semiaxes.

1 Introduction

The field of the electrokinetics of concentrated suspensions is still poorly understood. A complete description of the hydrodynamic and electrical interactions between disperse particles surrounded by a non-homogeneously charged atmosphere (the electric double layer, EDL) has not been achieved, despite the potential applicability of electrokinetic techniques to such systems. The problem has been approximately solved, using cell models, in the case of hard spherical particles.[1–4] Even more limited is our knowledge of the electrokinetics of nonspherical particles or with complex internal structures, although they can be found in many practical situations.[5,6]

The anisotropy associated to the non-spherical geometry gives rise to field-induced interactions which are responsible for the presence of either normal,[7] or anomalous[8–10] orientation with respect to the field. All these experiments were performed in conditions under which the electric double layers around particles are polarized, and the interactions between the induced dipoles are responsible for the observed behaviours.

In fact, the polarization state of colloidal particles manifests in most electrokinetic phenomena.[11] However, when a deep physical insight of polarization is required, as in the above mentioned situations, an analysis in the frequency domain offers much more information than the study of the electrokinetic quantities in the stationary state. In particular, the development of electroacoustic techniques,[12] and the recent advances in the determination of the low frequency permittivity of suspensions,[13] have provided us with very suitable tools. They are especially useful when the considered suspensions are concentrated and become turbid or even opaque, because optical determinations cannot be performed. Even the analysis of the polarization of dilute suspensions of non-spherical particles is a very challenging task,[14] and available literature has been almost absent until very recently. Some studies can be mentioned concerning the electrophoresis of spheroids,[15,16] or the electric permittivity of their suspensions,[17] but it has been only in the last years that the topic has gained attention and new theoretical treatments have appeared.[18–24] However, they are also limited to dilute conditions and a systematic experimental verification is lacking.

We have recently contributed a series of experimental results on the low frequency dielectric dispersion (LFDD) and dynamic electrophoretic mobility of moderately concentrated suspensions of rod-like colloids,[6,25–27] showing some of the effects that interactions have on the electrokinetic response investigated. In particular, we presented some unexpected behaviour of the LFDD spectra due to interactions between particles.[6] Our measurements suggest that the presence of neighbouring particles has little effect on the polarization along the symmetry axis of the particle, while it has strong effect on the perpendicular component. In order to clarify these observations, we present in this work new data on the LFDD and electroacoustics of moderately concentrated (up to 12% volume fraction of solids)

Department of Applied Physics, School of Sciences, University of Granada, 18071 Granada, Spain. E-mail: rul@ugr.es; Tel: +34-958243209
† Current address: Dipartimento di Medicina Sperimentale Facolta' di Medicina e Chirurgia, Universita' di Milano - Bicocca, Via Cadore 48, 20052 Monza (MB), Italy.

suspensions, and on their analysis in terms of the theoretical models that we developed in ref. 26,27.

The paper is organized as follows. A brief theoretical background is provided in section 2, stressing the role of the interactions. Section 3 describes the colloidal suspensions used in this work, as well as the two experimental techniques, namely, LFDD and electroacoustics, which allow us to analyse the polarization spectrum of colloidal particles in the range 1 kHz–18 MHz. The experimental results concerning the effects of the volume fraction of solids on the electrokinetic response of hematite particles are presented in section 4. The implications of the experimental results are discussed in section 5, and a justification for the observed behaviour based on the geometry of the concentration polarization clouds is proposed.

2 Electrokinetics of non-spherical particles

The description of the polarization of the double layer is often presented in terms of the dipole coefficient $\tilde{C}^*$, related to the dipole moment $\mathbf{d}^*$ (* denotes a complex quantity) induced by the alternating electric field $\mathbf{E}$ with frequency ω as follows:[28]

$$\mathbf{d}^*(\omega) = 3V\varepsilon_0\varepsilon_m\tilde{C}^*(\omega)\cdot\mathbf{E} \quad (1)$$

where $\tilde{C}^*(\omega)$ is a complex tensor and V is the particle volume, see Fig. 1. ε_0 and ε_m are the electric permittivity of vacuum and the relative electric permittivity of the medium, respectively. In the case of non-spherical particles, the analysis of the polarization is complicated by the fact that there is not a single characteristic dimension. Fortunately, because of the linearity of the problem, we can consider separately different components. In the frame of reference defined by the symmetry axes of the spheroid, the only non-zero components of the resulting diagonal tensor are $C^*_{\parallel}$ and $C^*_{\perp}$, respectively in directions parallel and perpendicular to the symmetry axis (Fig. 1). Hence:

$$d^*_i(\omega) = 4\pi\varepsilon_0\varepsilon_m ab^2 C^*_i(\omega)E_i \quad (2)$$

where d_i and E_i are i components ($\parallel$, $\perp$ to the axis of the spheroid) of the induced dipole and the field, and $2a$ ($2b$) is the symmetry axis (diameter) of the spheroid. The dipole coefficient carries all the information about the polarization processes that take place upon the application of the electric field,[13] and hence the values of the macroscopic quantities of the suspensions can be calculated from it.

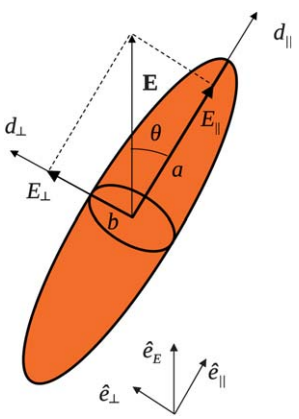

Fig. 1 Semiaxes a and b and components of the dipole and the field.

In the case of charged, hard colloidal particles, the frequency-spectrum of the dipole coefficient exhibits two main relaxations depending on which polarization processes can follow the field oscillations. These relaxations are called α and Maxwell–Wagner–O'Konski (MWO). The former takes place in the kHz region: when the frequency is above its characteristic relaxation frequency ω_α, concentration polarization cannot occur. This phenomenon gives rise to two clouds of perturbed ionic strength at the outer edge of the electric double layer, one with lower salt concentration than the bulk and other with higher salt concentration. It is originated by the fact that the transport numbers of cations and anions inside the EDL are different to their bulk values.[13] A sketch of the situation thus established is shown in Fig. 2. This process implies the transport of ions along distances of the order of the particle dimensions, and therefore its characteristic frequency can be estimated as the inverse of the time that these clouds need to disappear by diffusion, $\omega_\alpha = 1/\tau_\alpha \simeq D/L_D^2$, being L_D the diffusion length and D the diffusion coefficient

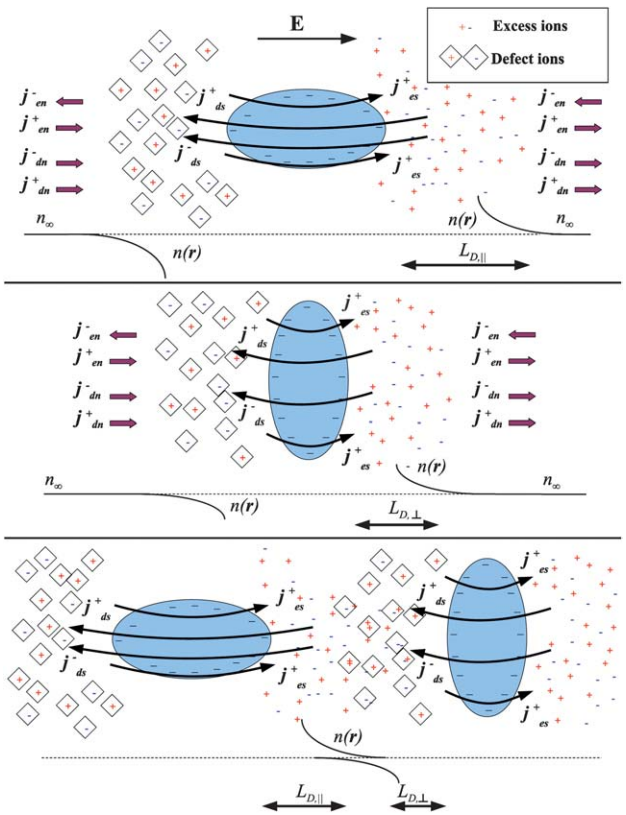

Fig. 2 Schematics of the electromigrational and diffusive fluxes in the vicinity of a spheroid oriented parallel (top) or perpendicularly (middle) to the field, and the way concentration polarization clouds of different particles overlap when two particles are close enough (bottom). This overlap leads to a partial cancellation of the perturbations on the ionic strength and the diffusive fluxes associated to them. $\mathbf{j}^{\pm}_{dn}$ ($\mathbf{j}^{\pm}_{en}$): diffusive (electromigrational) fluxes outside the EDL; $\mathbf{j}^{\pm}_{ds}$ ($\mathbf{j}^{\pm}_{es}$): diffusive (electromigrational) fluxes inside the EDL; $n(\mathbf{r})$: neutral electrolyte concentration outside the EDL; n_∞: neutral electrolyte concentration far from the EDL.

of the ions. In the case of non-spherical particles, we can distinguish two characteristic values of the diffusion length $L_{D,\parallel}$ and $L_{D,\perp}$, as illustrated in Fig. 2, and therefore two characteristic frequencies are expected.

The MWO relaxation takes place in the MHz region of the spectrum, and is a consequence of the mismatch of the values of the permittivity and conductivity of particles and medium. Above the characteristic frequency ω_{MWO}, the dipole coefficient depends on the permittivity of particles and medium, while its value is determined by their conductivities below ω_{MWO}. The characteristic distance is in this case of the order of the EDL thickness, κ^{-1}, and hence, the relaxation time can be estimated as $\tau_{\mathrm{MWO}} = 1/\omega_{\mathrm{MWO}} \simeq \kappa^{-2}/D$. Contrary to the case of α-relaxation, a single MWO process is expected also for rod-like particles, as it depends only slightly on size and shape.

These two processes modify the value of the dipole coefficient, and if they are sufficiently apart in the dielectric spectrum, three regions will be distinguished, separated by the two characteristic frequencies, ω_α and ω_{MWO}. Direct experimental access to the value of the dipole coefficient is not possible, and only indirect estimations can be made available based on the measurement of some electrokinetic quantity together with a theoretical model. In this work, we measured the spectra of the relative electric permittivity $\varepsilon^*(\omega)$ and the dynamic electrophoretic mobility $u_e^*(\omega)$ in suspensions of spheroidal nanoparticles. Their relationship to the dipole coefficient will be described below, while the electrokinetic theory that allows us to obtain the zeta potential and characteristic sizes of the particles from them is presented in Appendix A.

Distinguishing again parallel and perpendicular orientation of the spheroid ($i = \parallel, \perp$), the components of the relative permittivity of a dilute suspension and of the dipole coefficient of the particle are related as follows:[13]

$$\begin{aligned}\varepsilon_i^*(\omega) &= \varepsilon_m + \Delta\varepsilon_i^*(\omega) \\ &= \varepsilon_m\left(1 + 3\phi C_i^*(\omega)\right) - j\frac{3\phi K_m}{\omega\varepsilon_0}\left(C_i^*(\omega) - C_i^*(0)\right)\end{aligned} \quad (3)$$

where ϕ is the volume fraction of the suspension occupied by particles, K_m is the conductivity of the electrolyte solution and $j = \sqrt{-1}$. Here, we have defined the dielectric increment $\Delta\varepsilon_i^*(\omega)$, which accounts for the contribution of the dispersed particles to the electric permittivity of the suspension, and is the quantity experimentally accessible. It is also convenient to introduce its specific counterpart $\delta\varepsilon_i^*(\omega) = \Delta\varepsilon_i^*(\omega)/\phi$, the dielectric increment per unit volume fraction. These quantities are often expressed in terms of their real and imaginary components. For example:

$$\Delta\varepsilon_i^*(\omega) = \Delta\varepsilon_i'(\omega) - j\Delta\varepsilon_i''(\omega) \quad (4)$$

Concerning the dynamic electrophoretic mobility of a concentrated suspension of colloidal spheroids, it can be found through a version of the Helmholtz–Smoluchowski equation, where additional effects are accounted for by multiplying it by three functions:[26]

$$u_{e,i}^*(\omega) = \frac{\varepsilon_m\varepsilon_0\zeta}{\eta} f_i^1(\omega)\cdot f_i^2(\omega)\cdot f_i^3(\omega) \quad (5)$$

where η is the viscosity of the medium, typically water, and ζ is the zeta or electrokinetic potential. Here, $f_i^1(\omega)$ takes into account the particle inertia and is found from hydrodynamics,[16] $f_i^2(\omega)$ considers the EDL polarization, establishing the dependence with the dipole coefficient, and $f_i^3(\omega)$ carries information on particle concentration effects.

The inertia function $f_i^1(\omega)$ relaxes above a certain frequency $\omega_{in} \simeq \eta/\rho_m b^2$ (ρ_m is the density of the electrolyte solution) in the case of prolate spheroids. This frequency is strongly dependent on particle size. For higher frequencies, the particle and fluid cannot follow the fast inversions of the electric field and their mobility goes to zero.

$f_i^2(\omega)$ was first evaluated by Loewenberg and O'Brien[16,29–31] for $\kappa l_{min} \gg 1$, with l_{min} the minimum dimension of the spheroid. We write it in the following way, different to the original papers and also to our previous one,[26] but it is equivalent to them:

$$f_i^2(\omega) = (1 - L_i) - 3L_i(1 - L_i)C_i^*(\omega) \quad (6)$$

where L_i are the geometry-dependent depolarization factors. Expressions for them and for the function $f_i^1(\omega)$ are given in Appendix A.

The macroscopic values of these quantities are estimated as their averages, assuming random orientation:

$$\left\langle \varepsilon^*(\omega) \right\rangle = \frac{\varepsilon_\parallel^*(\omega) + 2\varepsilon_\perp^*(\omega)}{3} \quad (7)$$

$$\left\langle u_e^*(\omega) \right\rangle = \frac{u_{e,\parallel}^*(\omega) + 2u_{e,\perp}^*(\omega)}{3} \quad (8)$$

Brownian motion ensures a random distribution of the orientation if the interaction energy W between the induced dipole moment and the field itself verifies $W \ll k_B T$, where k_B is the Boltzmann constant and T is the temperature.[28] In the case of prolate spheroids:

$$\frac{\varepsilon_m\varepsilon_0 V E^2}{k_B T} \ll 1 \quad (9)$$

For a spheroid with $a = 300$ nm and $b = 60$ nm, this condition requires $E \ll 45$ kV m^{-1}. As we discuss below, although this condition is not always fulfilled, orientation effects are negligible in our experiments.

2.1 Consideration of particle–particle interactions

The presence of other particles in suspension has significant effects on the electrokinetic response of colloidal suspensions. Cell models[1–4] have demonstrated to be very suitable to account for such effects, but their application is limited to the case of spherical particles. There is not a model equivalent to the cell approach for the evaluation of particle interactions in suspensions of spheroids. It seems hence reasonable to use a phenomenological calculation which may allow us to gain a coherent interpretation of our data. The models used here were originally developed for spheres, one for the permittivity in the region of the spectra where the α-relaxation takes place[32] and the other for the dynamic mobility in the MWO relaxation,[33] and extended by us to be applicable to non-spherical particles.[6,26,27] The physical phenomenology associated to the interactions in the low frequency part of the spectrum, *i.e.*, where the α relaxation takes place, is richer and contains more information than the

interactions in the region of the MWO one, and therefore we focus our description on that relaxation.

The first model considers the overlap of concentration-polarization ionic clouds of different particles.[32] Such overlap has two effects on the spectrum of the dielectric permittivity. On one hand, when two particles are close enough, the ion-enriched region of one particle will partially balance the ion depleted region of its neighbour. This provokes partial cancellation of the perturbations of the local concentration and subsequent reduction of the fluxes that lead to the large values of the electric permittivity commonly observed at low frequency. On the other hand, the ionic diffusion lengths are shortened when particles approach each other, thus decreasing the characteristic time of the process, as shown in Fig. 2. In the dielectric spectrum, these effects lead to the presence of a local maximum in the $\Delta\varepsilon'(0) - \phi$ relation followed by a monotonous decrease, while $\omega_{\alpha,i}$ increases exponentially if $\phi \leq 0.6$.

The relationship between the specific dielectric increment at zero frequency and the characteristic α-relaxation frequency of a moderately concentrated suspension and of a dilute one can be described by the following expressions:[6,32]

$$\delta\varepsilon_{\alpha,i} = \delta\varepsilon^{d}_{\alpha,i}\left(1 + \frac{1}{(\phi_{\text{eff}}^{-1/3} - 1)^2}\right)^{-3/2} \tag{10}$$

$$\omega_{\alpha,i} = \omega^{d}_{\alpha,i}\left(1 + \frac{1}{(\phi_{\text{eff}}^{-1/3} - 1)^2}\right) \tag{11}$$

where the superscript ^{d} refers to the values in dilute conditions, and where we have introduced an "effective volume fraction" $\phi_{\text{eff}} = f \times \phi$, needed to properly fit our experimental results.[6] Here, f is a factor including information on the size and shape of the concentration polarization clouds, and therefore on the particle geometry. Note that f will also be different for each orientation of the particles with respect to the applied field.

As mentioned, the effect of the particle concentration on the dynamic mobility is taken into account through the function $f_i^3(\omega)$ in eqn (5). In this case we follow a model proposed by Ahualli *et al.*[33] accounting for hydrodynamic and electrical interactions between particles close to each other. Its predictions are in good agreement with more elaborate treatments explicitly dealing with interactions between pairs of particles[34] or based on cell models.[35] The function $f_i^3(\omega)$ in eqn (5) reads:[26]

$$f_i^3(\omega) = \frac{1 - \phi}{(1 - \phi C_i^*(\omega))(1 + \phi\Delta\rho/\rho_m)} \tag{12}$$

The numerator in this fraction comes from hydrodynamic interactions. The first factor in the denominator accounts for electrical interactions, while the term $(1 + \phi\Delta\rho/\rho_m)$ ensures that calculations are performed in the zero-momentum frame of reference, in accordance with existing experimental methods. $f_i^3(\omega)$ has little dependence on the frequency of the applied field, and it predicts a decrease in the magnitude of the mobility in the whole spectrum.

3 Materials and methods

The hematite particles were synthesized through hydrolysis of iron(III) chloride solutions at 100 °C as described in ref. 36. Their size and shape were characterized by dynamic light scattering (hydrodynamic radius $R_H = (130 \pm 30)$ nm) and SEM pictures (semiaxes $a = (276 \pm 18)$ nm and $b = (45 \pm 6)$ nm, so that $r = a/b = 6.1 \pm 1.2$, see Fig. 3). Prior to any analysis, the synthesized particles were cleaned by successive cycles of centrifugation and redispersion in deionized and filtered water (Milli-Q Academic, Millipore, France) until the conductivity of the supernatant was below 1 mS cm^{-1}.

In order to avoid the *suspension effect*[37,38] of the particles when measuring the pH, the preparation of the samples was as follows: once the suspension was clean, the centrifugation–redispersion procedure was repeated with a solution of the desired ionic strength and pH until they reach constant values in the supernatant. The volume of the final suspension was controlled to reach the highest concentration of solids. Suspensions with lower volume fractions were prepared by dilution.

The method used to measure the spectra of the electric permittivity consisted in the determination of the impedance of a parallel platinized-platinum electrode cell with variable cell constant.[39] The impedance was measured with an HP 4284A (USA) in the 1 kHz–2 MHz range. Typically, the applied electric field strength was 50 mV cm^{-1}, thus verifying the isotropy condition given by eqn (9). The main limitation when performing low-frequency impedance spectroscopy in aqueous media is the phenomenon of electrode polarization (EP), which may add a contribution to the measured impedance in the kHz frequency range, partially masking the signal coming from the particle-solution interface. Among other existing methods,[7,39] the *logarithmic derivative* technique has been shown to be able to reduce to a large extent the contribution of electrode polarization.[40,41] The logarithmic derivative of the real part of the relative permittivity, $\varepsilon'(\omega)$, is $\varepsilon''_D = -\pi/2(\partial\Delta\varepsilon'/\partial \ln \omega)$. This quantity displays a frequency dependence similar to that of the imaginary part of the electric permittivity ($\varepsilon''_D(\omega) \simeq \varepsilon''(\omega)$), but, interestingly, the electrode contribution to ε''_D‡ falls with frequency more rapidly than its contribution to ε'', and this makes it easier to eliminate or minimise the electrode polarization contribution.

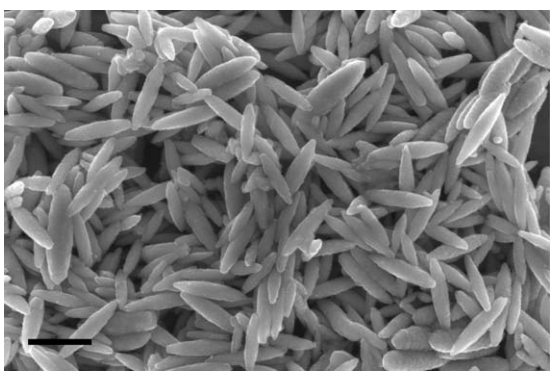

Fig. 3 The SEM picture of the synthesized hematite particles. Bar length: 500 nm.

‡ We must note here that the actual dependence in the relevant part of the spectrum is $\varepsilon''_D \propto \omega^{-2}$ instead of the usually interpreted $\varepsilon''_D \propto \omega^{-3/2}$. This issue will be discussed in a forthcoming contribution.

Furthermore, the real component of the permittivity can be obtained from it by numerical integration.

An example of the correction procedure is shown in Fig. 4, which shows the low-frequency dielectric spectrum of a suspension of hematite particles (12% volume fraction of solids). The upper panel corresponds to the logarithmic derivative ε''_D with and without the EP contribution. The real part, obtained by numerical integration of the corrected logarithmic derivative data, is depicted in the bottom panel. In this spectrum we observe two relaxation peaks at frequencies $\omega_{\alpha,\mathrm{LF}} \simeq 5$ kHz and $\omega_{\alpha,\mathrm{HF}} \simeq 300$ kHz. The spectra were fitted to the real part, and its logarithmic derivative, of a frequency dispersion function consisting of two Cole–Cole relaxations:[42]

$$\Delta\varepsilon^*(\omega) = \frac{\Delta\varepsilon_{\alpha,\mathrm{LF}}}{1+(j\omega/\omega_{\alpha,\mathrm{LF}})^{1-\gamma_{\mathrm{LF}}}} + \frac{\Delta\varepsilon_{\alpha,\mathrm{HF}}}{1+(j\omega/\omega_{\alpha,\mathrm{HF}})^{1-\gamma_{\mathrm{HF}}}} \qquad (13)$$

Here, $\omega_{\alpha,\mathrm{LF}}$ and $\omega_{\alpha,\mathrm{HF}}$ are the characteristic frequencies of the low- and high-frequency relaxations, respectively, whose amplitudes are expressed by the dielectric increments $\Delta\varepsilon_{\alpha,\mathrm{LF}}$ and $\Delta\varepsilon_{\alpha,\mathrm{HF}}$. $\gamma_{\mathrm{LF,HF}}$ are parameters of the respective Cole–Cole functions, indicating their width.

The experimental determination of the dynamic mobility was carried out by means of the electroacoustic technique known as ESA, or Electrokinetic Sonic Amplitude, based on the determination of the amplitude and phase of the sound wave generated in the colloidal suspension by application of an oscillating field in the frequency range 1 to 18 MHz. The device used is the Acoustosizer II (Colloidal Dynamics, USA), which is specially useful for the determination of the mobility in the region where the MWO relaxation and the inertia decrease are present.

The applied field depends on the sample properties, and in aqueous media it ranges between 1 kV m^{-1} and 12 kV m^{-1}, so that the condition given by eqn (9) that $E \ll 45$ kV m^{-1} is not verified in general. The strength of the field determines the degree of orientation in steady state, but not the time required to reach such average orientation. That time is related to the rotational diffusion coefficient, D_R, through the expression $\tau_R = 1/6D_R$; in our case, $\tau_R \simeq 5$ ms, much longer than the duration of the Acoustosizer pulses (a few μs[12]).

4 Results and discussion

4.1 General features of dielectric and electroacoustic spectra

The two relaxations observed in Fig. 4 correspond to the separate contributions of the EDL relaxations for parallel and perpendicular orientations, that is, the α-dispersions associated to each semiaxis of the spheroids.[6,25,27] Assuming random orientation of the particles, we identify:

$$\omega_{\alpha,\parallel} \equiv \omega_{\alpha,\mathrm{LF}} \qquad (14)$$

$$\omega_{\alpha,\perp} \equiv \omega_{\alpha,\mathrm{HF}} \qquad (15)$$

$$\Delta\varepsilon_{\alpha,\parallel} \equiv 3\Delta\varepsilon_{\alpha,\mathrm{LF}} \qquad (16)$$

$$\Delta\varepsilon_{\alpha,\perp} \equiv \frac{3}{2}\Delta\varepsilon_{\alpha,\mathrm{HF}} \qquad (17)$$

This interpretation was already proposed in a previous contribution,[25] where the characteristic frequencies of two α relaxations and the MWO one for dilute suspensions of the same particles where found to be $\omega_{\alpha,\parallel} \simeq 5$ kHz, $\omega_{\alpha,\perp} \simeq 50$ kHz and $\omega_{\mathrm{MWO}} \sim$ 4–6 MHz, with almost independence of ionic strength and pH. The value we find for $\omega_{\alpha,\parallel}$ is in agreement with previous experiments in dilute conditions, but $\omega_{\alpha,\perp}$ is about one order of magnitude larger in our case. As we show below, this disagreement on the $\omega_{\alpha,\perp}$ value is due to the effect of particle–particle interactions present in the LFDD experiments.

A spectrum of the dynamic mobility obtained from electroacoustics is shown in Fig. 5, which allows us to estimate the

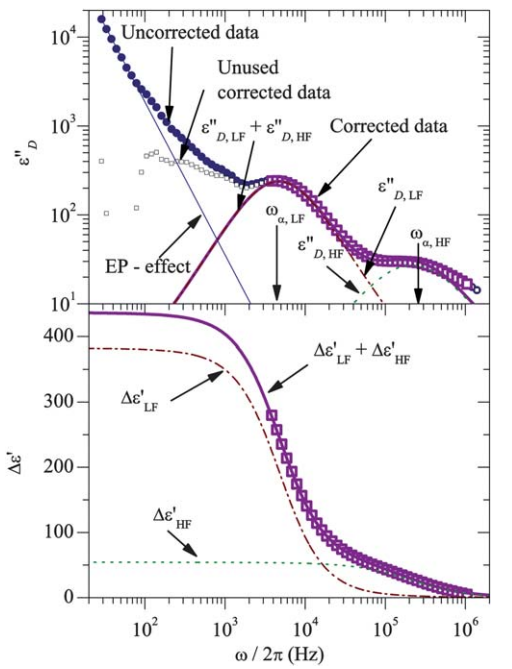

Fig. 4 Logarithmic derivative of the real part (top) and real part (bottom) of the dielectric increment of a 12% hematite suspension in a solution 0.5 mM of KNO_3 and pH = 3.7. Full circles: uncorrected data; open squares: EP-corrected data. The lines are the best-fit curves of a two Cole–Cole function to the corrected data. The characteristic frequencies of the two relaxations are identified as $\omega_{\alpha,\ \mathrm{LF}}$ and $\omega_{\alpha,\ \mathrm{HF}}$.

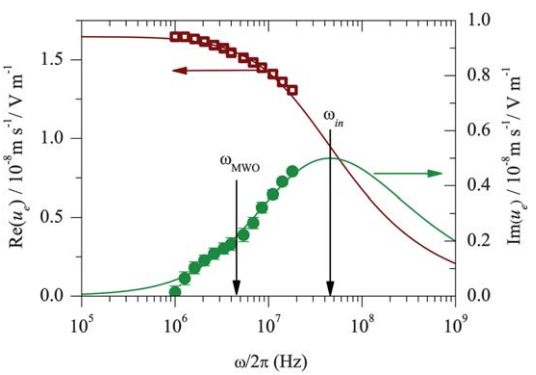

Fig. 5 Real (left) and imaginary (right) parts of the dynamic mobility spectrum of an 8% volume fraction hematite suspension in a 0.5 mM KNO_3 solution at pH 5.8. Vertical arrows indicate the approximate positions of ω_{MWO} and ω_{in}. Lines are fittings to the model (eqn (5)).

characteristic frequencies $\omega_{MWO} \simeq 5$ MHz and $\omega_{in} \simeq 50$ MHz. This value of ω_{MWO} is in agreement with the ones already referred to, and the inertia decay is found to be very similar to that theoretically expected for our particles, $\omega_{in} \simeq \eta/\rho_m b^2 \simeq 70$ MHz.

Therefore, we have found that the set of experimental results we obtain from the two experimental techniques used is coherent, providing information of the two α and the MWO relaxation processes, and the inertial decay. In the following, we analyse how solids contents affect the electrokinetic response of hematite suspensions, interpreting these effects with the described theoretical models.

4.2 Effects of ϕ on LFDD

We performed a set of LFDD experimental determinations in hematite suspensions with a wide range of ϕ values (2%–20%). This study was done in a KNO_3 0.5 mM solution at pH 3.7, experimental conditions under which the particles in suspension have a considerable (positive) surface charge.[25] Fig. 6 depicts the logarithmic derivative of the real part without the contribution of EP (top panel) and the real part (bottom panel) of the electric permittivity increment of such suspensions.

We observe that $\Delta\varepsilon_{\alpha,LF} \gg \Delta\varepsilon_{\alpha,HF}$. In fact, for the lowest values of ϕ the HF peak is almost undetectable, as it is completely masked by the LF one. However, the two maxima are better resolved the larger the particle concentration, due to their different tendencies. A quantitative description of the main features of these spectra is made possible by fitting the data to the logarithmic derivative of eqn (13). From the fittings, the parameters in Fig. 7 were obtained. Fig. 7(a) and Fig. 7(b) show the dielectric increments $\Delta\varepsilon_{LF,HF}$ and the specific dielectric increments ($\delta\varepsilon \equiv \Delta\varepsilon/\phi$), respectively, and Fig. 7(c) includes the characteristic frequencies of the Cole–Cole distributions. Note that, in the fitting procedure, it is not possible to discriminate between the two peaks for the lowest values of ϕ, since they are very close to each other. However, we found that all the curves where the two relaxations are well separated can be fitted with the values $\gamma_{LF} = 0.1$ and $\gamma_{HF} = 0.19$. We selected these two γ values for the whole data set and did not vary them.

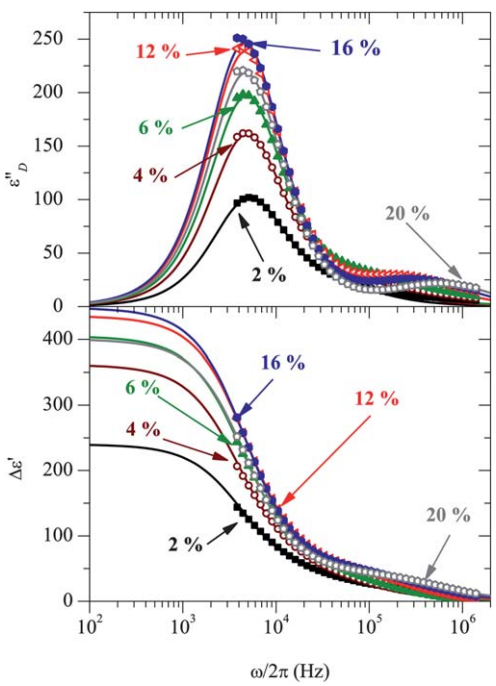

Fig. 6 Real part of the dielectric increment (bottom) and its logarithmic derivative (top) for concentrated hematite suspensions in 0.5 mM KNO_3 at pH = 3.7, and the indicated values of ϕ. Lines are fittings of a combination of two Cole–Cole relaxation functions.

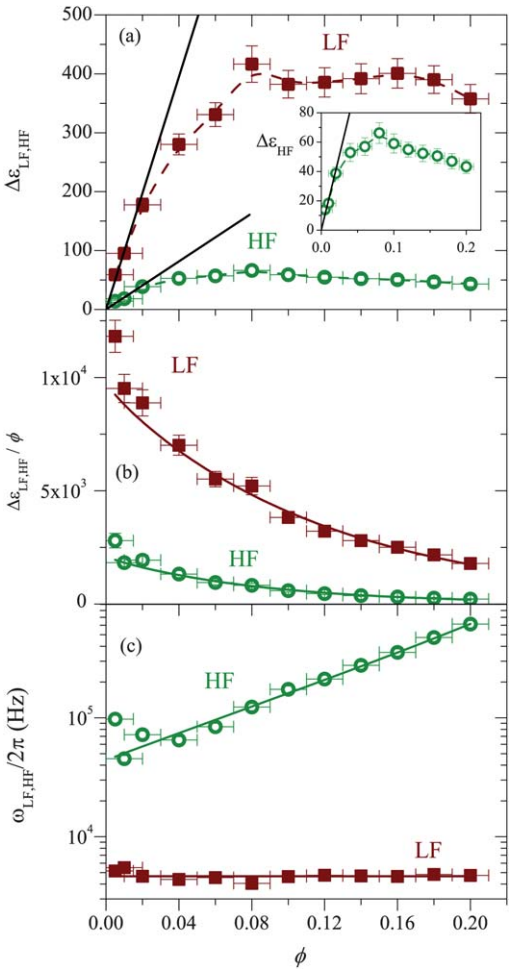

Fig. 7 Full squares: LF data. Open circles: HF data. (a) Value of the dielectric increment obtained from the fittings of data in Fig. 6 to eqn (13). Solid lines: fits to a linear model of the data with $\phi < 0.02$. Dashed lines are a guide to the eye. The inset is a zoom of the HF curve. (b) Value of the specific dielectric increment (symbols) and its fittings to eqn (10) (lines). (c) The same as (a), but for the values of the characteristic frequency. The lines here are the best fits to eqn (11).

The amplitude of the low-frequency (LF) relaxation process (Fig. 7a) goes through a maximum and reaches a plateau when the volume fraction of solids is increased. The amplitude of the high-frequency (HF) relaxation also describes a maximum, but beyond it the amplitude of the relaxation decreases. Moreover, the behaviours of the characteristic frequencies in the LF and HF cases are very different (Fig. 7c): while the former has a constant value $\omega_{LF} \simeq 5$ kHz, the HF one experiences an increase from $\omega_{HF} \simeq 40$ kHz to $\omega_{HF} \simeq 600$ kHz, that is, a shift of more than one decade.

Fig. 7(b) and (c) also include the best-fit lines of data to eqn (10) and 11, which allow us to obtain the dilute suspension parameters $\delta\varepsilon^d_{\alpha,i}$ and $\omega^d_{\alpha,i}$ (Table 1). According to data in Fig. 7, only the high frequency behaviour agrees qualitatively with the predictions of these equations. We can also consider the low volume fraction parts of $\Delta\varepsilon - \phi$ plots in Fig. 7(a). In this region, a linear dependence is found because the particles are far enough from each other as to make their interactions negligible. These linear ranges were fitted to an equation of the type $\Delta\varepsilon = \delta\varepsilon^d \times \phi$, and therefore the values of "$\delta\varepsilon^d_{\alpha,i}$" can be extracted, as indicated in Table 1 ("Linear region").

As we can see, the characteristic frequencies obtained for the α relaxations are now in good agreement with those obtained in dilute conditions,[25] thus confirming that the disagreement mentioned above is due to interaction effects. Finally, we can calculate the zeta potential by means of eqn (40) and 46 together with Bikerman equation, eqn (36) (see Appendix A.2). Using $\zeta_\parallel$ and $\zeta_\perp$, and the two characteristic sizes $L_{D,i}$ ($L_{D,\parallel} = a$ and $L_{D,\perp} = b$) as free parameters, we obtain the data shown in Table 2.

We find two clearly different values of the zeta potential, $\zeta_\parallel$ being considerably larger than $\zeta_\perp$. As a consequence, we also obtain two different values of the surface conductivity, and that associated to the parallel orientation is larger than the perpendicular one. The estimated value for b is quite close to the actual one (45 nm), while the value of a is three times larger than that obtained by electron microscopy. We could argue that this disagreement is due to a likely aggregation between particles, responsible for a larger diffusion length and therefore returning a smaller characteristic frequency. To clarify this, we analyse below simultaneously the LFDD and the electroacoustic response (suitable to accurately determine the size of the particles) of suspensions of hematite at a higher pH (5.8), closer to the isoelectric point (pH $\simeq$ 7[25]), where aggregation would be more likely present, due to the lower surface charge.

4.3 Comparison of LFDD and ESA data

We carried out both types of measurements (LFDD and ESA) in suspensions with varying values of the concentration of particles (in the range 2%–12%), always in 0.5 mM KNO_3 solutions at pH 5.8. These results are depicted in Fig. 8. Note that the two dielectric increments (LF and HF) are very similar, as theoretically predicted.[17] In both cases, we see that $\Delta\varepsilon_\alpha$ increases with the solid contents until reaching a maximum at $\phi = 0.08$. Although the highest value here is $\phi = 0.12$ and the tendencies after the maxima are not clear, we can say that, in agreement with the case pH = 3.7 (Fig. 6 and 7): (*i*) $\Delta\varepsilon_{\alpha,\mathrm{HF}}$ decreases when we change ϕ from 0.10 to 0.12, and we also see the concomitant increase of $\omega_{\alpha,\mathrm{HF}}$; (*ii*) $\Delta\varepsilon_{\alpha,\mathrm{LF}}(\phi = 0.10) \simeq \Delta\varepsilon_{\alpha,\mathrm{LF}}(\phi = 0.12)$, and $\omega_{\alpha,\mathrm{LF}}$ is not affected by ϕ in the analysed range. Therefore, it seems reasonable to expect that these parameters will follow a trend with ϕ compatible with that observed in the case pH = 3.7.

Table 1 Best-fit parameters of the data in Fig. 7 to eqn (10) and 11, and to the equation $\Delta\varepsilon(\phi) = \delta\varepsilon^d \times \phi$. $f_{\delta\varepsilon}$ and f_ω are the f values obtained by fitting the data of $\delta\varepsilon_\alpha$ and ω_α, respectively

	$\delta\varepsilon^d_{\alpha,i}$	$f_{\delta\varepsilon}$	$\delta\varepsilon^d$ (Linear region)
LF	9900 ± 400	1.06 ± 0.04	9900 ± 400
HF	2130 ± 120	1.47 ± 0.06	2040 ± 140
	$\omega^d_\alpha/2\pi$ (kHz)	f_ω	
LF	4.66 ± 0.23	—	
HF	43 ± 4	2.42 ± 0.15	

Table 2 Characteristic time and diffusion length of the α relaxation, and zeta potential, for each orientation of the symmetry axis of the particle with the field. The surface conductivity K^σ_i was obtained assuming that all its contribution comes from that calculated with the Bikerman equation[43]

	$\tau_{\alpha,i}$/μs	$L_{D,i}$/nm	ζ_i	$K^\sigma_i/10^{-9}$ S
∥	34 ± 2	971 ± 15	136 ± 1	1.84 ± 0.04
⊥	3.7 ± 0.2	52 ± 4	28 ± 1	0.046 ± 0.003

Using the same treatment of LFDD experiments as in the case of pH = 3.7, we obtain the parameters in Table 3. The characteristic frequencies of the α processes coincide with those obtained from the pH = 3.7 data, thus confirming that they are little affected by the surface potential. However, the dielectric increments are considerably lower, since they strongly depend on pH through the zeta potential.

Table 4 is obtained following the same procedure to calculate the parameters as in Table 2, but for the data at pH = 5.8. The characteristic times and lengths of the α relaxations are equal to the values obtained at pH 3.7, as their dependence with surface charge is negligible. However, the zeta potential and surface conductivity are considerably lower than in the previous case, as expected from the pH value.

The dynamic mobility spectra, displayed on the right hand side of Fig. 8, exhibit the well known decreasing tendency of the dynamic mobility with ϕ due to electrical and hydrodynamic interactions between particles. The region of the spectra experimentally accessible contains the MWO relaxation ($\omega_{\mathrm{MWO}} \simeq$ 5 MHz) and the beginning of the inertial decay. In the imaginary part of the mobility (plotted on the bottom-right of Fig. 8) we observe that both processes are better distinguished when ϕ increases. This is a consequence of the fact that the MWO relaxation process is less affected by interactions than the inertial decrease. When ϕ is raised the amplitude of the inertial decay is diminished, whereas the MWO relaxation remains unaffected, this making it more apparent.

From the fittings of these spectra to the model, also shown in Fig. 8, we obtain the parameters in Table 5. We observe that, for the specified confidence intervals, a single value of the zeta potential suffices to fit all the spectra, confirming the validity of this model, in which the assumption of no EDL overlap is used. However, the value of the size parameter b slightly decreases as the volume fraction of solids increases. Note that this behaviour must be the consequence of the limited frequency range accessible, since the only expected tendency would be an increase of the particle size due to aggregation, which would lead to *smaller* characteristic frequencies. Hence, we will take averages of the obtained values of $\bar{\zeta} = 39 \pm 3$ mV and $\bar{b} = 47 \pm 9$ nm, and consider them as representative of moderately concentrated suspensions of hematite particles at the used ionic strength and pH.

It seems of interest to consider the comparison of the parameters obtained from the two experimental techniques, LFDD and electroacoustics. From dielectric spectroscopy, we obtain in both

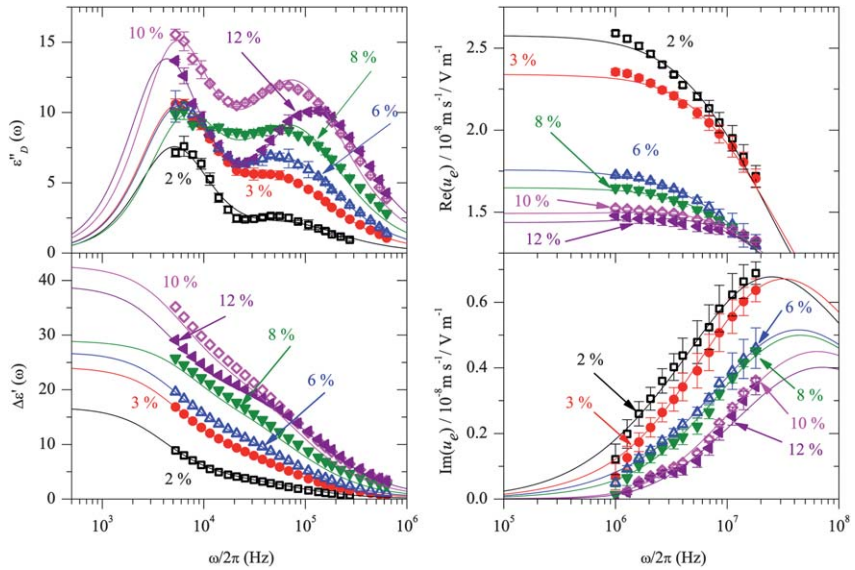

Fig. 8 Symbols: dielectric (left) and electroacoustic (right) spectra of suspensions of hematite particles in a KNO_3, 0.5 mM solution at pH = 5.8 for the indicated values of ϕ. Lines are fittings of the real part of eqn (13) and its logarithmic derivative (left) and of the dynamic mobility (real and imaginary parts) to models.

Table 3 Best-fit parameters of the dielectric increment data in Fig. 8 to eqn (10) and 11. $f_{\delta\varepsilon}$ and f_ω are the f values obtained by fitting the data of $\delta\varepsilon_\alpha$ and ω_α, respectively

	$\delta\varepsilon^{\,d}_{\alpha,i}$	$f_{\delta\varepsilon}$	$\omega^d_\alpha/2\pi$ (kHz)	f_ω
LF	820 ± 70	2.2 ± 0.1	5.4 ± 0.9	—
HF	720 ± 130	2.3 ± 0.3	50 ± 4	1.16 ± 0.02

Table 4 As Table 2, but for the experiments at pH 5.8 (parameters in Table 3)

	$\tau_{\alpha,\,i}$/μs	$L_{D,i}$/nm	ζ_i/mV	$K_i^\sigma/10^{-9}$ S
∥	30 ± 6	860 ± 90	69 ± 2	0.31 ± 0.02
⊥	3.2 ± 0.3	51 ± 2	18 ± 2	0.017 ± 0.013

Table 5 Best-fit parameters of the electroacoustic data in Fig. 8 to the dynamic mobility calculated from the model

ϕ	ζ/mV	b/nm
0.02	42 ± 3	61 ± 5
0.03	42 ± 1	54 ± 3
0.06	35 ± 3	47 ± 5
0.08	38 ± 1	44 ± 3
0.10	39 ± 3	61 ± 3
0.12	40 ± 5	37 ± 4

cases (pH 5.8 and 3.7) two very different values of the zeta potentials ($\zeta_\parallel$ and $\zeta_\perp$), which are also considerably different from the value obtained from electroacoustics. Note that the presence of a non-uniform zeta potential is likely to occur considering that the equipotential surface in spheroidal geometry is not at constant distance to the spheroidal surface, while the ideal stagnant (electrokinetic) plane most likely is. However, a simple average can suggest that these differences are not that important, as $\bar{\zeta} = (\zeta_\parallel + 2\zeta_\perp)/3 \simeq 35$ mV is very similar to the zeta potential deduced from electroacoustics. Jimenez *et al.*[25] justified the necessity of different zeta potentials arguing the existence of a non-negligible Stern layer conductivity. This assumption was based on the differences between the zeta potentials obtained from low and high frequency dielectric spectroscopy, and with DC electrophoresis data. In fact, rigorous calculations have recently shown that Stern layer conduction added to the classical diffuse layer contribution strongly influences the dielectric behaviour of colloidal suspensions, but have little impact on electrophoretic mobility.[44] Therefore, this additional conductivity could be also responsible for the disagreements observed in our experiments.

Regarding our estimations of the characteristic diffusion lengths $L_{D,i}$, it is remarkable the precision reached in the determination of the correct value of the short semiaxis with both LFDD and electroacoustics, in spite of the number of assumptions made in the development of the theoretical model. On the contrary, the dimension of the long semiaxis obtained from LFDD is approximately three times larger than observed in SEM and light scattering. Considering that aggregation is not plausible in our system, the large diffusion lengths in the parallel direction could well be the manifestation of a finite Stern layer conductivity or of non-homogeneous zeta potential distribution.

5 Consideration of concentration polarization clouds

Perhaps the most unexpected finding presented is how the contents of solids affects (or better, how it does not affect) the characteristic frequency of the LF α-relaxation. The proved (both theoretically and experimentally[2,32,45]) increase in α-frequency with ϕ in the case of spheres (and in the perpendicular orientation of our particles) is completely absent in the LF relaxation peak, giving in turn a zero value for the parameter f.

Note that this cannot be explained by assuming that the volume fraction is low so that the particles are far from each other on average, as we observe an effect on the dielectric increment.

As previously mentioned, we consider that the suspensions are overall isotropic. It could be argued that the presence of either pre-nematic fluctuations of a nematic phase[46] can explain the different effects of ϕ on the LF and HF relaxation processes, through lateral interactions between the particles. While the presence of ordered clusters cannot be ruled out, the volume fractions of the suspensions investigated are far from the typical values reported for the occurrence of the nematic phase.[47] Hence, the eventual alignment that might appear in the form of fluctuating nematic domains cannot significantly affect our results. We propose that the presented data can be explained without assuming the presence of such ordering phenomena. Alternatively, a careful examination of the concentration polarization clouds obtained from the theoretical model by Grosse, Pedrosa and Shilov[17,48] allows us to justify the observed behaviour based on the geometry of these clouds. Using eqn (49) and 50 in the Appendix, we plotted the lines of equal increment of ionic strength due to concentration polarization as shown in Fig. 9 (similar plots were obtained for parallel orientation in ref. 21). The two plots are, respectively, the extreme situations of electric field oriented parallel and perpendicular to the symmetry axis of the spheroid, and any intermediate situation will be an appropriate combination of these two. The lines represent the geometrical locus of equal normalized increment of ionic strength $\delta\bar{n}$ (see figure caption). The $\delta\bar{n}$ step between each two consecutive iso-lines is constant, and therefore the gradients of salt concentration are larger where the iso-lines are closer, as usual.

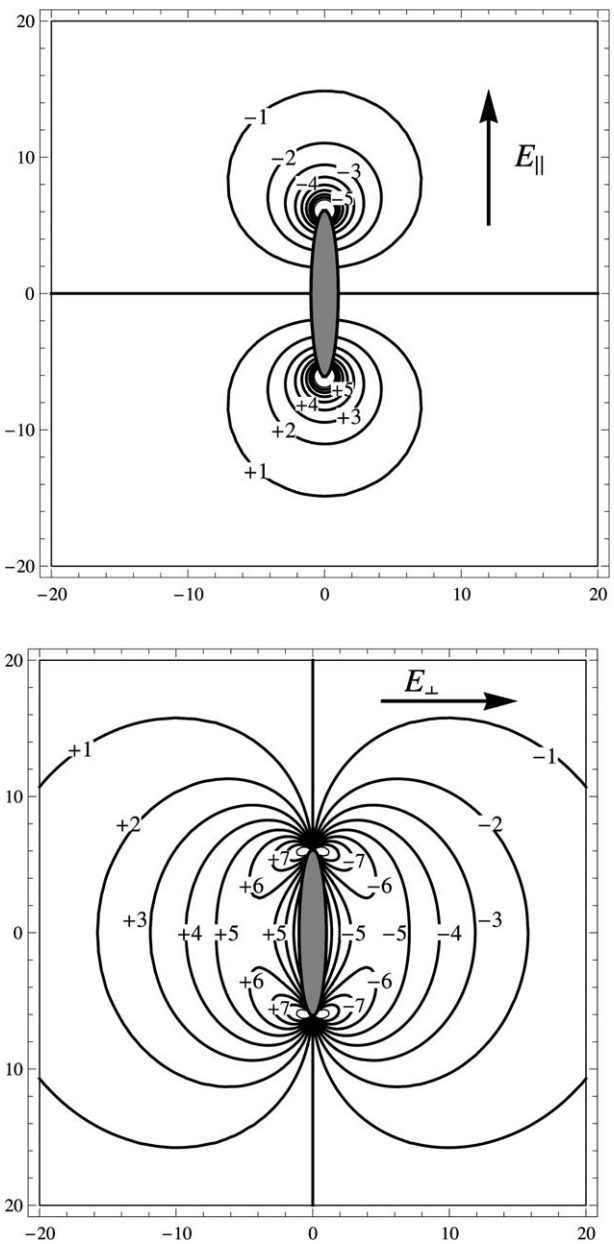

Fig. 9 Lines of equal value of the normalized increase of the ionic strength $\delta\bar{n} = 10^7 \delta n/n_\infty E$ for the parallel (upper panel) and perpendicular (lower panel) components of the applied field with respect to the symmetry axis of the spheroids. Ordinates and abscissas are given in units of b. Used values: $b = 45$ nm, $r = 6.1$, 0.5 mM KNO_3, $\zeta = 100$ mV.

From these plots, we can clearly see that the regions of neutral electrolyte perturbed by concentration polarization are much larger in the perpendicular case than in the parallel one, and that the regions of significant perturbation in the latter orientation are localized very close to the tips of the spheroids. Therefore, reaching a significant overlap of the concentration polarization regions close to the ends of the particles will require quite short distances between particles, shorter than expected in our experiments, given the volume fractions of solids studied. On the contrary, the extensive perturbation of the component perpendicular to the symmetry axis will lead to very likely interactions in that direction.

Therefore, the f parameter includes information not only on the distance between the surfaces of different particles, but also on the internal structure of the suspension (if any) and the size and shape of the concentration polarization clouds. These considerations justify the large differences on the obtained values of f, also revealing the difficulties that their appropriate interpretation imply.

6 Conclusions

In this work, a wide set of experimental results have been presented, which allowed us to characterize the AC electrokinetic response of moderately concentrated suspensions of prolate hematite particles. The use of an approximate model provides a coherent interpretation of the observed behaviour and makes it possible to estimate the zeta potential and the size and geometry of the suspended particles.

In the low frequency region of the spectrum, LFDD experiments reveal the presence of two α relaxations, associated with the two characteristic sizes of the particles. The main interactions in this frequency range are due to the overlap of the regions outside the EDL with perturbed ionic strength due to concentration polarization. At the examined values of particle concentration, the asymmetry of the concentration polarization clouds justifies the different trends of the two α relaxations with the volume fraction of solids.

A Summary of theory

A.1 Inertia function

The inertia term in eqn (5) can be written in terms of the drag coefficient D^i_{H} and added mass M^i_a:[16]

$$f^1_i = \frac{D^i_{\mathrm{H}} - j\omega M^i_a}{D^i_{\mathrm{H}} + j\omega M} \tag{18}$$

For a not very elongated spheroid ($0.1 < r < 10$, $r = a/b$):[49]

$$D^i_{\mathrm{H}} = -\eta l_i \left[F^i_0 + \lambda_i B_i + (\lambda_i)^2 \frac{M^i_a}{\rho_m l_i^3} + \left(\frac{(F^i_0)^2}{6\pi} - B_i \right) \frac{\lambda_i}{1+\lambda_i} \right] \tag{19}$$

where

$$\lambda_i = (1-j)\sqrt{\frac{\omega l_i^2 \rho_m}{2\eta}} \tag{20}$$

Here, l_i is the minimum dimension of the particle in a direction perpendicular to its motion (hence to the field); in the case of prolate spheroids, l_i is the short semiaxis for both orientations. The expression of the added mass in terms of the *depolarization coefficients*:

$$L_{\parallel} = \begin{cases} \dfrac{1}{1-r^2} + \dfrac{r}{(r^2-1)^{3/2}} \ln\left(r + (r^2-1)^{1/2} \right) & r > 1 \\ \dfrac{1}{1-r^2} - \dfrac{r}{(1-r^2)^{3/2}} \cos^{-1} & r < 1 \end{cases} \tag{21}$$

$$L_{\perp} = \frac{1 - L_{\parallel}}{2} \tag{22}$$

is:

$$M^i_a = \rho_m V m^i_a = \rho_m V \frac{L_i}{1 - L_i} \tag{23}$$

with m^i_a the dimensionless added mass. The Stokes resistance reads:

$$F^{\parallel}_0 = \frac{8\pi r}{1 + L_{\parallel}(2r^2 - 1)} \tag{24}$$

$$F^{\perp}_0 = \frac{8\pi a/l_i}{r^2 - L_{\perp}(2r^2 - 3)} \tag{25}$$

and the Basset force:

$$B_i = \frac{H_i}{l_i^2 (1 - L_i)^2} \tag{26}$$

where:

$$H_i = \frac{4\pi}{3} a b^2 g_i \tag{27}$$

For prolate spheroids ($h = \sqrt{a^2 - b^2}$, being $2h$ the focal distance):

$$g_{\parallel} = \frac{3a}{2bh} \left(\frac{a^2 - 2b^2}{h^2} \arctan \frac{h}{b} + \frac{b}{h} \right) \tag{28}$$

$$g_{\perp} = \frac{3a}{2bh} \left(\frac{a^2}{2h^2} \operatorname{arccot} \frac{b}{h} + \frac{b(a^2 - 2b^2)}{2a^2 h} \right) \tag{29}$$

A.2 Electrokinetic model for the dipole coefficient

The simplest description of the frequency spectrum of the dipole coefficient, including the two relevant relaxation mechanisms (α and MWO), can be expressed as the superposition of two Debye-type relaxations:

$$C^*_i(\omega) = C^{\infty}_{\mathrm{MWO},i} + \frac{C^0_{\mathrm{MWO},i} - C^{\infty}_{\mathrm{MWO},i}}{1 + j\omega\tau_{\mathrm{MWO},i}} + \frac{C^0_{\alpha,i} - C^{\infty}_{\alpha,i}}{1 + j\omega\tau_{\alpha,i}} \tag{30}$$

where $C^0_{\mathrm{MWO},i}$ and $C^{\infty}_{\mathrm{MWO},i}$ represent the low and high frequency limits of the dipole coefficient given by the MWO theory, respectively, while $C^0_{\alpha,i}$ and $C^{\infty}_{\alpha,i}$ are the limiting values of the α relaxation. Note that $C^{\infty}_{\alpha,i} = C^0_{\mathrm{MWO},i}$.

The results of approximate models in the case of thin EDL ($\kappa a \gg 1$ y $\kappa b \gg 1$) are briefly described below.

A.2.1 High frequency: MWO. Dukhin and Shilov[50] showed that the following limiting values of the dipole coefficient and the characteristic frequencies of the MWO relaxation constitute a good approximation to the exact numerical solution:

$$C^*_{\mathrm{MWO},i}(\omega) = C^{\infty}_{\mathrm{MWO},i} + \frac{C^0_{\mathrm{MWO},i} - C^{\infty}_{\mathrm{MWO},i}}{1 + j\omega\tau_{\mathrm{MWO},i}} \tag{31}$$

$$\tau_{\mathrm{MWO},i} = \varepsilon_0 \frac{(1 - L_i)\varepsilon_m + L_i \varepsilon_p}{(1 - L_i)K_m + L_i K_{p,i}} \tag{32}$$

$$C^{\infty}_{\mathrm{MWO},i} = \frac{\varepsilon_p - \varepsilon_m}{3(\varepsilon_m + (\varepsilon_p - \varepsilon_m)L_i)} \tag{33}$$

$$C^0_{\mathrm{MWO},i} = \frac{K_{p,i} - K_m}{3(K_m + (K_{p,i} - K_m)L_i)} \tag{34}$$

being

$$K_{p,i} = K^{\sigma} g_i \tag{35}$$

where K^{σ} is the surface conductivity, obtained from the Bikerman equation,[43] which for a binary electrolyte reads:

$$K^{\sigma} = K^{\sigma+} + K^{\sigma-} \tag{36}$$

$$K^{\sigma+} = \frac{2z^2 e^2 n_{\infty}}{\kappa k_B T} D^+ \left(\exp\left(-\frac{ze\zeta}{2k_B T} \right) - 1 \right) \left(1 + \frac{3m^+}{z^2} \right) \tag{37}$$

$$K^{\sigma-} = \frac{2z^2 e^2 n_{\infty}}{\kappa k_B T} D^- \left(\exp\left(\frac{ze\zeta}{2k_B T} \right) - 1 \right) \left(1 + \frac{3m^-}{z^2} \right) \tag{38}$$

Here, e is the elecron charge, z is the valence of the ions, n_{∞} is the ionic strength in the bulk, $D^{\pm}$ are the diffusion coefficients of cations and anions, and $m^{\pm}$ are the dimensionless mobility coefficients of ions:

$$m^{\pm} = \frac{2\varepsilon_m \varepsilon_0}{3\eta D^{\pm}} \left(\frac{k_B T}{e} \right)^2 \tag{39}$$

A.2.2 Low frequency: α relaxation. The approach that we follow was elaborated by Grosse, Pedrosa and Shilov, based on the free energy stored in the suspensions because of the concentration polarization.[17,48,51] It is assumed that the double layer is thin everywhere, ζ is moderately high and convection is negligible. The final expressions, useful for the calculation of the permittivity spectra, are shown here. The low-frequency dielectric increments read:

$$\delta\varepsilon_{\alpha,i}(0) = \frac{3\varepsilon_m\kappa^2}{16\pi ab^2}(\gamma_i^+ - \gamma_i^-)^2 I_i \tag{40}$$

where, for prolate spheroids, I_i can be written as:

$$I_\parallel = \frac{3\pi}{5h^6}\left(- a^3b^2\ln^2\frac{a+h}{a-h} + 2hb^2(a^2+b^2)\ln\frac{a+h}{a-h} + 4ah^2(a^2-2b^2)\right) \tag{41}$$

$$I_\perp = \frac{3\pi}{20h^6}\left(- ab^4\ln^2\frac{a+h}{a-h} + 4h(a^4+h^4)\ln\frac{a+h}{a-h} - 4ah^2(3a^2-2b^2)\right) \tag{42}$$

The $\gamma_i^\pm$ functions are:

$$\gamma_i^\pm = \frac{ab^2}{3}\frac{K_{p,i}^\pm - K_m/2}{K_m/2 + (K_{p,i}^\pm - K_m/2)L_i} \tag{43}$$

and the conductivities $K_{p,\,i}^\pm$:

$$K_{p,i}^\pm = g_i K^{\sigma\pm} \tag{44}$$

It will be also useful to have an expression for the induced dipole coefficient:

$$C_{\alpha,i}^0 = \frac{1}{2ab^2}(\gamma_i^+ + \gamma_i^-) \tag{45}$$

The characteristic time τ_α is found to be:

$$\tau_{\alpha,i} \simeq \frac{\delta\varepsilon_{\alpha,i}(0)}{3\varepsilon_m(C_{\alpha,i}^\infty - C_{\alpha,i}^0)}\tau_m \tag{46}$$

where $\tau_m = \varepsilon_0\varepsilon_m/K_m$ is the relaxation time of the electrolyte.

In the case of prolate spheroids a simple analysis of eqn (46) permits to obtain the following approximate relationships between the characteristic times and the diffusion length in each orientation:[17]

$$\tau_{\alpha,\parallel} \propto \frac{L_{D,\parallel}^2}{2D} \propto \frac{a^2}{2D} \tag{47}$$

$$\tau_{\alpha,\perp} \propto \frac{L_{D,\perp}^2}{2D} \propto \frac{b^2}{2D}\ln\frac{a}{b} \tag{48}$$

Finally, the expressions for the increments of the salt concentration outside the EDL due to concentration polarization are given by:

$$\frac{\delta n_\parallel}{n_\infty} = \frac{eE}{2k_BT}(\gamma_\parallel^+ - \gamma_\parallel^-)\frac{3Q_1(\cosh\chi)\cos\vartheta}{h^2} \tag{49}$$

$$\frac{\delta n_\perp}{n_\infty} = -\frac{eE}{2k_BT}(\gamma_\perp^+ - \gamma_\perp^-)\frac{3Q_1^1(\sinh\chi)\sin\vartheta\cos\xi}{2h^2} \tag{50}$$

where χ, ϑ and ξ are the spheroidal coordinates. The functions $Q_1(x)$ and $Q_1^1(x)$ are:

$$Q_1(x) = x\left(\frac{1}{2}\ln\frac{x+1}{x-1}\right) - 1 \tag{51}$$

$$Q_1^1(x) = \frac{\sqrt{x^2-1}}{2}\ln\frac{x+1}{x-1} - \frac{x}{\sqrt{x^2-1}} \tag{52}$$

Acknowledgements

Financial support from Junta de Andalucía (Spain) project PE-2008-FQM3993 is gratefully acknowledged. R.A.R. acknowledges MICINN (Spain) for an FPU grant and Regione Lombardia (Ricerca Applicata with ESF). M.L.J. also acknowledges the MICINN for her contract supported by Ramón y Cajal program.

References

1 S. Kuwabara, *J. Phys. Soc. Jpn.*, 1959, **14**, 527–532.
2 F. Carrique, F. J. Arroyo, M. L. Jiménez and A. V. Delgado, *J. Chem. Phys.*, 2003, **118**, 1945–1956.
3 F. Carrique, J. Cuquejo, F. Arroyo, M. Jiménez and A. Delgado, *Adv. Colloid Interface Sci.*, 2005, **118**, 43–50.
4 E. K. Zholkovskij, J. H. Masliyah, V. N. Shilov and S. Bhattacharjee, *Adv. Colloid Interface Sci.*, 2007, **134–135**, 279–321.
5 K. J. Lee, J. Yoon and J. Lahann, *Curr. Opin. Colloid Interface Sci.*, 2011, **16**, 195–202.
6 R. A. Rica, M. L. Jiménez and A. V. Delgado, *Soft Matter*, 2011, **7**, 3286–3289.
7 K. Kang and J. K. G. Dhont, *Soft Matter*, 2010, **6**, 273–286.
8 F. Mantegazza, M. Caggioni, M. L. Jiménez and T. Bellini, *Nat. Phys.*, 2005, **1**, 103–106.
9 I. Dozov, E. Paineau, P. Davidson, K. Antonova, C. Baravian, I. Bihannic and L. J. Michot, *J. Phys. Chem. B*, 2011, **115**, 7751–7765.
10 M. L. Jiménez, L. Fornasari, F. Mantegazza, M. C. D. Mourad and T. Bellini, *Langmuir*, 2012, **28**, 251–258.
11 A. V. Delgado, F. González-Caballero, R. J. Hunter, L. K. Koopal and J. Lyklema, *J. Colloid Interface Sci.*, 2007, **309**, 194–224.
12 R. J. Hunter, *Colloids Surf., A*, 1998, **141**, 37–66.
13 C. Grosse and A. V. Delgado, *Curr. Opin. Colloid Interface Sci.*, 2010, **15**, 145–159.
14 M. L. Jiménez and T. Bellini, *Curr. Opin. Colloid Interface Sci.*, 2010, **15**, 131–144.
15 R. W. O'Brien and D. N. Ward, *J. Colloid Interface Sci.*, 1988, **121**, 402–413.
16 M. Loewenberg and R. W. O'Brien, *J. Colloid Interface Sci.*, 1992, **150**, 158–168.
17 C. Grosse, S. Pedrosa and V. N. Shilov, *J. Colloid Interface Sci.*, 1999, **220**, 31–41.
18 M. Fixman, *J. Chem. Phys.*, 2006, **124**, 214506.
19 C. Chassagne and D. Bedeaux, *J. Colloid Interface Sci.*, 2008, **326**, 240–253.
20 H. Zhao and H. H. Bau, *Langmuir*, 2008, **24**, 6050–6059.
21 H. Zhao and H. H. Bau, *Langmuir*, 2010, **26**, 5412–5420.
22 J. K. G. Dhont and K. Kang, *Eur. Phys. J. E*, 2010, **33**, 51–68.
23 J. K. G. Dhont and K. Kang, *Eur. Phys. J. E*, 2011, **34**, 40.
24 G. Manning, *Eur. Phys. J. E*, 2011, **34**, 39.
25 M. L. Jiménez, F. J. Arroyo, F. Carrique and U. Kaatze, *J. Phys. Chem. B*, 2003, **107**, 12192–12200.
26 R. A. Rica, M. L. Jiménez and A. V. Delgado, *Langmuir*, 2009, **25**, 10587–10594.
27 R. A. Rica, M. L. Jiménez and A. V. Delgado, *J. Colloid Interface Sci.*, 2010, **343**, 564–573.

28 L. Landau and E. Lifshitz, *Electrodynamics of continuous media*, Pergamon Press, 1984.
29 M. Loewenberg, *Phys. Fluids A*, 1993, **5**, 765–767.
30 M. Loewenberg, *Phys. Fluids A*, 1993, **5**, 3004–3006.
31 M. Loewenberg, *J. Fluid Mech.*, 1994, **278**, 149–174.
32 A. V. Delgado, F. J. Arroyo, F. González-Caballero, V. N. Shilov and Y. B. Borkovskaya, *Colloids Surf., A*, 1998, **140**, 139–149.
33 S. Ahualli, A. V. Delgado and C. Grosse, *J. Colloid Interface Sci.*, 2006, **301**, 660–667.
34 R. W. O'Brien, A. Jones and W. N. Rowlands, *Colloids Surf., A*, 2003, **218**, 89–101.
35 S. Ahualli, A. Delgado, S. J. Miklavcic and L. R. White, *Langmuir*, 2006, **22**, 7041–7051.
36 M. P. Morales, T. González-Carreño and C. J. Serna, *J. Mater. Res.*, 1992, **7**, 2538–2545.
37 S. Oman, M. Camoes, K. Powell, R. Rajagopalan and P. Spitzer, *Pure Appl. Chem.*, 2007, **79**, 67–79.
38 S. Oman, M. Camoes, K. Powell, R. Rajagopalan and P. Spitzer, *Pure Appl. Chem.*, 2007, **79**, 81–86.
39 M. C. Tirado, F. J. Arroyo, A. V. Delgado and C. Grosse, *J. Colloid Interface Sci.*, 2000, **227**, 141–146.
40 P. A. Cirkel, J. P. M. van der Ploeg and G. J. M. Koper, *Phys. A*, 1997, **235**, 269–278.
41 M. L. Jiménez, F. J. Arroyo, J. van Turnhout and A. V. Delgado, *J. Colloid Interface Sci.*, 2002, **249**, 327–335.
42 K. Cole and R. Cole, *J. Chem. Phys.*, 1941, **9**, 341–351.
43 J. J. Bikerman, *Kolloid-Z.*, 1935, **72**, 100–108.
44 F. Carrique, F. J. Arroyo, V. N. Shilov, J. Cuquejo, M. L. Jiménez and A. V. Delgado, *J. Chem. Phys.*, 2007, **126**, 104903.
45 S. Ahualli, M. L. Jiménez, A. V. Delgado, F. J. Arroyo and F. Carrique, *IEEE Trans. Dielectr. Electr. Insul.*, 2006, **13**, 657–663.
46 S. Chandrasekhar, *Liquid Crystals*, Cambridge University Press, Cambridge, 1992.
47 G. J. Vroege and H. N. W. Lekkerkerker, *Rep. Prog. Phys.*, 1992, **55**, 1241–1309.
48 C. Grosse and V. N. Shilov, *J. Colloid Interface Sci.*, 1997, **193**, 178–182.
49 C. J. Lawrence and S. Weinbaum, *J. Fluid Mech.*, 1988, **189**, 463–489.
50 S. S. Dukhin and V. N. Shilov, *Adv. Colloid Interface Sci.*, 1980, **13**, 153–195.
51 C. Grosse, *Ferroelectrics*, 1988, **86**, 171–179.